Progress In Electromagnetics Research, PIER 9, 219–263, 1994

MICROWAVE CHIRAL MATERIALS: A REVIEW OF EXPERIMENTAL STUDIES AND SOME RESULTS ON COMPOSITES WITH FERROELECTRIC CERAMIC INCLUSIONS

F. Guérin

1. Introduction

Chirality has enjoyed an increasing interest in the last ten years. The subject is not new and has been investigated since the 19^{th} century, mostly in chemistry. However, novel concepts such as "electromagnetic chirality" or "microwave chirality", referring to the study of the interaction of a handed material with an electromagnetic wave which frequency belongs to the RF, microwave or millimetric ranges, have been introduced and developed. What was a few decades ago a minor branch is now becoming a growing field of research. On the theoretical side, a large volume of publications is available. This does not mean that all phenomena related to electromagnetic chirality are well understood, but subsequent progress has been made. On the contrary, little was done on the experimental side. Despite the lack of results, two patents were granted in 1990 and 1992. One deals with chiral composites for shielding and absorption [1], while the other focuses on the use of chiral media in waveguides [2]. Each of these patents is related to one of the two families of applications foreseen for chiral materials: electromagnetic coatings and microwave or optronic components and devices. These two important domains perhaps justify the recent interest electromagnetic chirality has benefited from.

Interestingly enough, the study of chiral substances started in the beginning of the last century with an experimental breakthrough, the discovery of optical rotatory dispersion by Arago and Biot in certain categories of solids, liquids, and gases. Fresnel then explained this phenomenon, generally referred to as circular birefringence, by the existence of different refractive indices for right and left circularly polarized light in such materials, termed optically active. Around 1850, a crucial step was accomplished by Pasteur as he shed light on the link between optical activity and the existence of structural asymmetry, an expression soon replaced by the word chirality. Another experimental step was achieved by Cotton in 1895 with the discovery of circular dichroism, or unequal absorption of right and left circularly polarized light, also due to chirality. Finally, at the beginning of the 20^{th} century, the situation could be summarized as follows: the interaction of light with chiral, or handed, media produces both circular birefringence and dichroism (Fig. 1). In the following decades, much of the work was dedicated to understanding optical activity on a molecular basis within the formalism of quantum chemistry. The first tentative effort to examine the

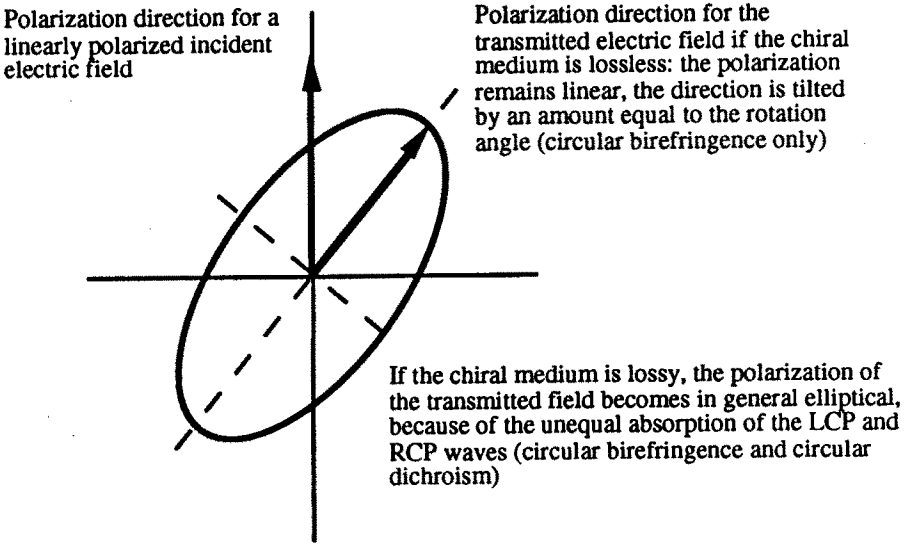

Figure 1. Illustration of circular birefringence and dichroism occurring in a chiral medium (RCP and LCP stand for right circularly polarized and left circularly polarized, respectively).

possible occurrence of macroscopic optically active objects was made in 1914 by Lindman. In a 1920 paper, he reported the measurement of the polarization rotation of a linearly polarized wave after propagating through a medium consisting of copper springs randomly embedded in cotton balls [3]. The springs had a stretched length L of 9 cm, a diameter D of 10 mm and 2.5 turns. The measurements were carried out at wavelengths comprised between 12.2 and 34.2 cm (frequencies ranging from 0.88 to 2.46 GHz). Lindman found a critical wavelength λ_o at which a resonance occurred in the frequency behavior of the polarization rotation angle, and was able to link this result to the stretched length of the springs via the formula $\lambda_o = 2L$ (a corresponding critical frequency f_o can also be defined). He also demonstrated that media comprising right–handed and left–handed springs exhibited opposite rotations, as well as the fact that the composites behaved isotropically as far as rotation was concerned. In 1956, the results were contested

by Winkler, who attributed them to anisotropic scattering rather than true optical activity [4]. However, the following year, Tinoco and Freeman observed rotatory dispersion and circular dichroism for arrays of copper helices, after carefully checking their equipment against scattering effects [5]. They used wavelengths ranging from 2.1 to 3.6 cm (frequencies ranging from 8.33 to 14.29 GHz), while their helices had a stretched length L of 4.7 cm, a diameter D of 0.5 cm and three turns. They found a good agreement between the experimental results for the rotatory dispersion α of their samples and the Drude–type law

$$\alpha = \sum_j \frac{k_j}{\lambda^2 - \lambda_j^2} \tag{1}$$

where λ is the wavelength of the exciting field, k_j are real coefficients and $\lambda_j = 2L/j$, j being an integer. This study helped establish unambiguously the concept of electromagnetic activity, generalizing to lower frequencies the phenomenon of optical activity, commonly observed at optical and infra–red frequencies. At the same time, it appeared clear that a chiral object was most active for wavelengths related to its dimensions, and that a scale effect existed: for a chiral object to exhibit sufficient activity, the wavelength of the exciting field should be roughly comparable to its size (by this we do not mean equal, but neither too large, nor too small).

More than three decades passed between Tinoco and Freeman's first paper and the next experimental report by Guire, Varadan and Varadan [6]. The chiral samples studied were 2.7 cm thick composites made of a random dispersion of copper–coated stainless steel helices in an epoxy resin. The helices were subsequently smaller than in the previously mentioned studies: their diameter D was 1.32 mm, the pitch was 0.53 mm and they had 3 turns. By means of a microwave free–space set–up operating between 14.5 and 17.5 GHz, the reflection coefficient of short–circuited samples of various concentration was measured. The underlying idea behind this, which had been investigated theoretically earlier [7], was to elaborate chiral coatings susceptible of decreasing reflections from metallic surfaces. Similar composites were prepared by Umari, Varadan, and Varadan and tested in the 12–18 GHz range with the same free–space set–up as above [8]. Several metal concentrations from 0.4 % to 3.2 % in volume were considered. The circular birefringence and dichroism of the samples were investigated. It was checked that composites containing springs of opposite handedness exhibited

opposite rotations, while racemic composites (containing right–handed and left–handed helices in equal amounts) behaved effectively as achiral or non–chiral materials. The rotation angle was found to be independent of frequency, which can be attributed to the narrowness of the frequency range of observation, and proportional to the volume fraction of the inclusions. Other results on the transmission characteristics of metal–epoxy chiral composites in the 8–40 GHz range were reported by Ro, Varadan, and Varadan [9]. To our knowledge, the most complete study on the properties of composites with metallic springs was made by Ro. He undertook the determination of the effective constitutive parameters of such materials [10], especially the third variable quantifying chirality (usually called chirality parameter or coefficient). He contributed to refining measurement procedures, and proposed a method for computing the electromagnetic properties of chiral media from values of S-parameters measured by means of a free–space system. Some attempts to characterize chiral composites consisting of a dispersion of copper–coated stainless steel helices in silicone rubber have also been made by Hollinger, Varadan, Ghodgaonkar, and Varadan using circular waveguides [11]. The Cotton effect, referring to the rotation angle changing sign along with the circular dichroism reaching an extremum in a narrow frequency range, has been observed in the C band (5.85–8.2 GHz). It was shown that the critical frequency f_o at which the phenomenon occurs was concentration dependent: f_o was decreased if the inclusion volume fraction was increased. Besides the fact that results agree well with those obtained for similar materials using free–space techniques, it is interesting to note that circular birefringence and dichroism resonance effects depend not only on the size of the inclusions, but also on their concentration. In order to elaborate composites with a given value of f_o, it may therefore be possible to use inclusions of a size smaller that what the desired value of f_o would have prescribed, provided that their loading rate is high enough. Finally, some experimental work has recently been initiated in Europe, in particular in France and Finland.

A common feature to those of the previously mentioned studies relative to microwave chirality, is that composites were always made of metallic springs embedded in a relatively low–loss matrix. Such a composition is easy to elaborate, since no particular processing technique is required for fabricating either the inclusions or the matrix. However, it may not give sufficient freedom for designing materials with

prescribed properties. For instance, a chiral composite with metallic inclusions cannot have too high a spring loading if it is to be used for reflection reduction, since it would most likely act as a reflecting surface. For applications requiring low insertion losses, metallic helices may not be suitable either. We have therefore chosen to investigate alternate ways for producing chiral materials, and decided to work with ceramic helices as chiral inclusions. Intuitively, it appears that by simply changing the nature of the ceramic material or modifying its composition, one can reach a broader range of characteristics than by using metals. Ceramics encompass such a wide range of physical properties – dielectric, magnetic, piezoelectric, or semiconductive, to name a few – that they are a particularly versatile class of materials. Other features of ceramic materials, such as their high temperature stability and, for some categories of ceramics, the dependence of one or several of their properties with respect to an external force or field, seemed also attractive. Among the various possibilities, we selected a high permittivity ferroelectric ceramic as our inclusion material.

In the following, we first focus on the equations governing EM wave propagation in a chiral continuum. Various microwave characterization methods susceptible of being used are reviewed and the free–space normal incidence method is presented in some detail. We also indicate how material properties can be computed from reflection and transmission measurements. Then, we present the fabrication stage; in particular, the process used for fabricating ferroelectric ceramic helices is described and results on microstructural characterization are presented. In the third part, experimental results are given and discussed. Finally, we evoke both experimental and theoretical problems that remain to be solved, and some possible directions for future research.

2. Interaction between an EM Wave and a Chiral Medium

2.1 Wave Propagation in a Chiral Continuum

A bi–isotropic medium being, in general, both chiral and non–reciprocal, can be described using the Drude–Born–Fedorov formalism

by the following set of constitutive equations [12]

$$\begin{cases} \vec{D} = \varepsilon\vec{E} + \varepsilon\alpha\nabla \times \vec{E} \\ \vec{B} = \mu\vec{H} + \mu\beta\nabla \times \vec{H} \end{cases} \tag{2}$$

The four quantities ε , $\mu, \alpha,$ and β are in general complex scalars. When compared with the situation for an isotropic dielectric and magnetic material, two additional parameters, α and β are needed to describe such a medium completely. They are called chirality parameters and have the dimension of length. If the medium is reciprocal, it is usually referred to by the expressions chiral medium or Pasteur medium. In this particular case, α and β are equal, so that only three constitutive parameters remain. Other sets of constitutive equations are acceptable, which are equivalent for time–harmonic fields. For example, in the Post–Jaggard formalism one would write for a Pasteur medium [13,14]

$$\begin{cases} \vec{D} = \varepsilon_p\vec{E} + \mathrm{i}\xi\vec{B} \\ \vec{B} = \mu_p\left(\vec{H} - \mathrm{i}\xi\vec{E}\right) \end{cases} \tag{3}$$

where ξ is called chirality admittance, while using Sihvola and Lindell's notation, one would define a general bi–isotropic medium by [15]

$$\begin{cases} \vec{D} = \varepsilon_b\vec{E} + (\chi - \mathrm{i}\kappa)\sqrt{\varepsilon_o\mu_o}\vec{H} \\ \vec{B} = \mu_b\vec{H} + (\chi + \mathrm{i}\kappa)\sqrt{\varepsilon_o\mu_o}\vec{E} \end{cases} \tag{4}$$

where chirality is quantified by the dimensionless parameter κ and non–reciprocity is introduced via χ, dimensionless as well. The relative merit of either formalism is a matter of debate; various constitutive equations are currently used by the different groups involved in microwave chirality research. In the rest of this article, we follow the Drude–Born–Fedorov (DBF) formalism and we restrict our analysis to chiral or Pasteur media, for which only one chirality parameter β is needed. The three material parameters $\varepsilon = \varepsilon' + \mathrm{i}\varepsilon''$, $\mu = \mu' + i\mu''$, and $\beta = \beta' + \mathrm{i}\beta''$ are taken to be complex. We also use a time dependence of the form $\mathrm{e}^{-\mathrm{i}\omega t}$ for the various fields throughout this article.

Using Maxwell's equations along with (2) and $\alpha = \beta$, a wave propagation equation can be found

$$\nabla^2\vec{E} + 2\beta\kappa^2\nabla \times \vec{E} + \kappa^2\vec{E} = \vec{0} \tag{5}$$

where κ is defined by $\kappa^2 = k^2/\left(1-(k\beta)^2\right)$ and $k = \omega(\varepsilon\mu)^{1/2}$. k is here a mere notation, it does not represent any wave propagation in the chiral substance. A linear transformation of the fields can be used to simplify (5)

$$\begin{cases} \vec{E} = \vec{Q}_L + a_R \vec{Q}_R \\ \vec{H} = a_L \vec{Q}_L + \vec{Q}_R \end{cases} \tag{6}$$

with $a_R = -\mathrm{i}(\mu/\varepsilon)^{1/2} = -\mathrm{i}\eta$ (the definition of the intrinsic impedance of a chiral medium is formally the same as for a non–chiral medium in the DBF formalism), and $a_L = -1/a_R$. Equation (6) involves two new fields $\vec{Q}_L$ and $\vec{Q}_R$, respectively left and right circularly polarized (LCP and RCP), and is known as the Bohren decomposition [16]. These fields allow for a simpler description of wave propagation in a chiral medium when compared to (5), since they both satisfy uncoupled Helmholtz equations

$$\begin{cases} \nabla^2 \vec{Q}_L + k_L^2 \vec{Q}_L = \vec{0} \\ \nabla^2 \vec{Q}_R + k_R^2 \vec{Q}_R = \vec{0} \end{cases} \tag{7}$$

where the LCP and RCP wavenumbers, respectively k_L and k_R, are given by

$$k_L = \frac{k}{1-k\beta}, \qquad k_R = \frac{k}{1+k\beta} \tag{8}$$

In the non–chiral limit, i.e., $\beta = 0$, k_L and k_R reduce to k. Equation (8) shows that for a non-vanishing chirality parameter, LCP and RCP waves propagate with different phase velocities and undergo different attenuations in a lossy chiral medium, causing circular birefringence and dichroism. The latter phenomena can be further quantified by writing $k_L = k_L' + \mathrm{i}k_L''$ and $k_R = k_R' + \mathrm{i}k_R''$, and computing the rotation angle θ along with the circular dichroism ξ associated with the transmission of a normally incident linearly polarized wave through a chiral slab of thickness d

$$\theta = \frac{(k_L' - k_R')\,d}{2} \qquad \text{and} \qquad \xi = \frac{(k_L'' - k_R'')\,d}{2} \tag{9}$$

An alternate way for quantifying circular dichroism is to define the ellipticity $\tan\gamma$ via $\tan\gamma = \tanh\xi$. The ellipticity is a measure of the ratio of the minor axis to the major axis of the transmitted wave

polarization ellipse. It is dimensionless, equal to 0 for the case of a linear polarization (no circular dichroism), and its magnitude is equal to 1 for the extreme case of a circular polarization (maximum circular dichroism).

Equation (8) can be rewritten in order to express k and β as a function of k_R and k_L, which can be useful for determining the chirality parameter from k_R and k_L measurements

$$\beta = \frac{1}{2}\left(\frac{1}{k_R} - \frac{1}{k_L}\right), \quad k = \frac{2}{\dfrac{1}{k_R} + \dfrac{1}{k_L}}, \quad \text{and } k\beta = \frac{k_L - k_R}{k_L + k_R} \tag{10}$$

We note that for the lossless case ($k_R'' = k_L'' = 0$), k and β are real. If we further assume a weak chirality ($k\beta \ll 1$), we have the relationship

$$\beta \approx \frac{\theta}{d}\left(\frac{1}{k}\right)^2 = \frac{\theta}{d\omega^2\varepsilon\mu} \tag{11}$$

Thus, if an estimate for ε and μ is known, a simple measure of the rotatory power θ/d at a given frequency leads to an estimate for the chirality parameter.

2.2 A Brief Review of Microwave Characterization Methods

Because the description of chirality requires a third constitutive parameter β, special methods must be employed for fully characterizing Pasteur media. With the past experimental results on optically active substances in mind, one intuitively realizes that some information on the polarization of an EM wave transmitted through a chiral sample must be sought. This remark prescribes techniques involving coaxial transmission lines, for the reason that a fixed polarization reference direction is needed. However, when only information on the magnitude of reflection coefficients are needed, such as for reflectivity studies, coaxial test fixtures of a diameter adapted to the microstructure of the material to be measured can be considered.

As mentioned in the introduction, an attempt to use a circular waveguide, which to the knowledge of the author is the first of its kind, was made by Hollinger et al. in the C band (5.85– 8.2 GHz) [11]. Composites comprising metallic helices in silicone rubber were tested. The method allowed only for the determination of the rotation angles

and axial ratios (reciprocal of the ellipticity) of the samples. General theoretical work on wave propagation in waveguides filled with chiral materials has been carried out recently [17,18], and a large amount of articles is now devoted to this topic. The principles of characterization techniques in waveguides have been investigated for bi-isotropic media [19]. Also considered was the possibility of using resonator techniques [20]. Although it is too early to know whether these methods will be of practical use, they seem to be attractive for measuring those chiral substances that may be employed in electronic devices.

The first and still the only existing method that has yielded complete experimental results on the properties of chiral materials, is the free–space technique. Past experiments using normal incidence illumination have already been evoked in the introduction [6, 8–10]. In this study, the technique used is similar to that of Ro [10] and will be described in detail in Sections 2.4. and 2.5. Such a technique is used at the Pennsylvania State University, USA and at IRCOM, University of Limoges, France. It should be added that another technique involving bistatic measurements is also in use at Penn State, and that a similar free–space method has recently been implemented in France [21].

2.3 Reflection and Transmission of Plane Waves

In this section, we consider a linearly polarized electromagnetic wave normally incident along the positive z direction on a chiral slab of thickness d and infinite lateral dimensions suspended in free–space (Fig. 2a). The slab is regarded as homogeneous and isotropic. The free–space wavenumber is k_o and the free–space impedance is η_o. The incident fields are

$$\begin{cases} \vec{E}_o = E_o e^{ik_o z} \vec{e}_y \\ \vec{H}_o = \dfrac{-E_o}{\eta_o} e^{ik_o z} \vec{e}_x \end{cases} \tag{12}$$

The E and H fields in the slab can be derived using Eq. (7), then (6). Their general form is a superposition of RCP and LCP waves propagating with respective wavenumbers k_R and k_L in the positive and negative z directions. The transmitted fields can be written as

$$\begin{cases} \vec{E}_t = (E_{tx}\vec{e}_x + E_{ty}\vec{e}_y)\, e^{ik_o z} \\ \vec{H}_t = \frac{1}{\eta_o}\,(-E_{ty}\vec{e}_x + E_{tx}\vec{e}_y)\, e^{ik_o z} \end{cases} \tag{13}$$

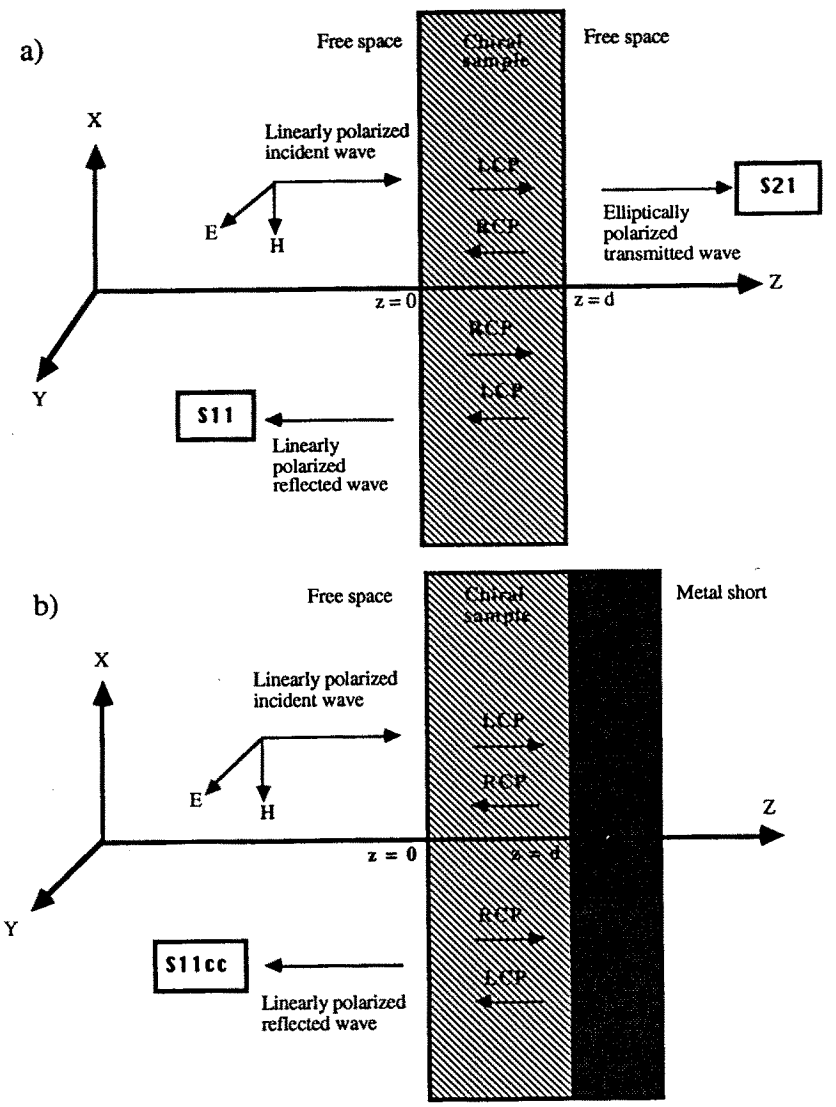

Figure 2. Interaction of a linearly polarized normally incident EM wave with a chiral slab and a metal–backed chiral slab.

while the reflected fields are

$$\begin{cases} \vec{E}_r = (E_{rx}\vec{e}_x + E_{ry}\vec{e}_y)\,\mathrm{e}^{-\mathrm{i}k_o z} \\ \vec{H}_r = \frac{1}{\eta_o}(E_{ry}\vec{e}_x - E_{rx}\vec{e}_y)\,\mathrm{e}^{-\mathrm{i}k_o z} \end{cases} \tag{14}$$

The unknown transmitted and reflected field coefficients are derived by enforcing the electric and magnetic fields boundary conditions at $z = 0$ and $z = d$. In this particular normal incidence case, the reflected field is found to be copolarized with the incident field, whereas the transmitted field has both copolarized and a crosspolarized components. Writing

$$\Psi = \mathrm{e}^{2\mathrm{i}k_L d},\ \Phi = \mathrm{e}^{\mathrm{i}(k_R - k_L)d},\ \text{and}\ \Gamma = \frac{\eta - \eta_o}{\eta + \eta_o} \tag{15}$$

the scattering parameters S_{11} and S_{21} of the slab, which can be regarded as the reflection and transmission coefficients as far as the copolarized parts of the fields are concerned, are found to be

$$\begin{cases} S_{11} = \dfrac{\Gamma(1 - \Phi\Psi)}{1 - \Gamma^2\Phi\Psi} \\ S_{21} = \dfrac{1 + \Phi}{2}\dfrac{\Psi^{1/2}\left(1 - \Gamma^2\right)}{1 - \Gamma^2\Phi\Psi} \end{cases} \tag{16}$$

By setting β equal to 0, we check that Eqs. (16) reduce to the case of a non–chiral slab. We also verify that (16) agree with the results obtained by Bassiri et al. [22] with constitutive relations (3).

The case of a metal–backed homogeneous and isotropic chiral slab (Fig. 2b) can be treated similarly by enforcing the electric and magnetic fields boundary conditions at $z = 0$, as well as the electric field boundary conditions at $z = d$. The reflection coefficient for a short–circuited chiral sample can be written as

$$S_{11}^{sc} = \frac{\Gamma - \Phi\Psi}{1 - \Gamma\Phi\Psi} \tag{17}$$

where Γ, Φ, and Ψ are given by (15). We also check that setting β equal to 0 yields the case of a regular dielectric and magnetic material.

In the following, we show how the measurement of reflection and transmission coefficients can be used for characterizing a chiral medium. With our method, the knowledge of the metal–backed reflection coefficient is not needed. Still, since it is a piece of information

regarding the normal incidence reflectivity of the samples, it is usually measured and stored for further comparison with results obtained from computer simulations.

2.4 The Free–Space Normal Incidence Method

The free–space bench used for testing chiral samples has already been described in the literature and was previously applied to dielectric and magnetic measurements at ambient temperature [23, 24], as well as to dielectric measurements at high temperature [25]. Because full details regarding the basic measurement procedure for chiral materials have been given by Ro [10], we should only review rapidly the principal features of the system. The main components of the circuitry are two spot–focusing horn lens antennas, one used for emission, the other for reception, which allow one to work with chiral samples in which active regions are as small as 4 in $\times$ 4 in. Originally, five frequency bands were available to us: the C (5.85–8.2 GHz), X (8.2–12.4 GHz), Ku (12.4–18 GHz), K (18–26.5 GHz), and Ka bands (26.5–40 GHz). Now the system is being upgraded at IRCOM so that a full 5.6–110 GHz coverage will soon be effective. A two–port TRL (Thru, Reflect, Line) calibration is performed in each band. It should be pointed out that because of the nature of the transitions used for feeding the antennas (rectangular and circular waveguides), each frequency band is studied separately. Time domain gating is systematically performed after each S-parameter acquisition. In general, measurements corresponding to at least four positions of the chiral sample in the holder are averaged in order to take into account non–uniformities due to the fabrication.

For fully characterizing chiral materials, three independent complex scalars are needed. We first record the reflection and transmission coefficients S_{11} and S_{21} with the receiving and the transmitting antennas in copolarized position, the analytical expressions of which were given in Eqs. (16). Then we record the transmission coefficient $S_{21\alpha}$ after the polarization direction of the receiving antenna was rotated about the optical axis of the system by an angle α (measured with respect to the polarization direction of the transmitting antenna). This third procedure essentially permits to obtain complete information on the polarization ellipse of the transmitted wave. With S_{21} given in (16) and S_{21cr} defined as the transmission coefficient for the crosspolarized

case, one can write

$$S_{21\alpha} = \cos\alpha S_{21} + \sin\alpha S_{21cr} \tag{18}$$

which allows for the determination of S_{21cr}. Once S_{11}, S_{21}, and S_{21cr} are known, the reflection and transmission coefficients for a RCP or a LCP wave incidence are calculated via

$$\begin{cases} S_{11}^{L} = S_{11}^{R} = S_{11} \\ S_{21}^{L} = S_{21} - \mathrm{i}S_{21cr} \\ S_{21}^{R} = S_{21} + \mathrm{i}S_{21cr} \end{cases} \tag{19}$$

where the superscripts L and R stand for LCP and RCP, respectively. The three quantities S_{11}, S_{21}^{R}, and S_{21}^{L} are then used for computing the various properties of interest.

2.5 Material Parameters Computation

The LCP and RCP transmission coefficients are used for computing the variable Φ defined in Eqs. (15). Then, the rotation angle θ and the ellipticity $\tan\gamma$ are deduced with

$$\begin{aligned} \theta &= \frac{(k'_L - k'_R)\,d}{2} = -\frac{1}{2}\arg(\Phi), \text{ and} \\ \tan\gamma &= \tanh\left(\frac{(k''_L - k''_R)\,d}{2}\right) = \tanh\left(\frac{\ln|\Phi|}{2}\right) \end{aligned} \tag{20}$$

where arg denotes the argument comprised between $-\pi$ and π. There is, in principle, $a \pm 2n\pi$ uncertainty, n being an integer, in the determination of $\arg(\Phi)$, which could be experimentally solved by testing two samples of the same material with different thicknesses, or by testing two samples, one being chiral, the other not, having the same thickness. However, all experiments conducted at Penn State and IR-COM on thin, low concentration, chiral samples (thickness typically ranging from one millimeter to one inch), whether the inclusions are metallic or dielectric, have yielded values of the rotation angle smaller than 180 degrees in magnitude, so that practically, it is sufficient for us to use the relationship given in (20).

The variable Φ being known, Ψ can be expressed as a function of Γ via the expression of S_{11} in (16) and replaced in the expression

of S_{21}^L to yield a quadratic equation in Γ. This equation is solved by imposing $|\Gamma| < 1$, which means that the reflection coefficient of a semi-infinite chiral medium is smaller than 1 in magnitude. The impedance η of the chiral medium is then computed with $\dot{\eta} = \eta_o(1+\Gamma)/(1-\Gamma)$. Using the expressions of Φ and Ψ in Eqs. (15), k_R and k_L can be obtained. There is, in this case, a true uncertainty in the determination of the real parts of the two wavenumbers. It can be solved by using the time–domain features of the HP 8510 network analyzer: the idea is to measure the average propagation delay time through the sample and deduce an approximate phase velocity, which is then used for estimating an average propagation constant and choosing the right values of the arguments of Φ and Ψ. Once k_R and k_L have been computed, it is verified that $k'_L > 0$, $k'_R > 0$, $k''_R \geq 0$, and $k''_L \geq 0$. β and k are then calculated with Eqs. (10). Finally, ε and μ are obtained using

$$\varepsilon = \frac{k}{\omega\eta} \qquad \text{and} \qquad \mu = \frac{k\eta}{\omega} \tag{21}$$

The method just explained is directly applicable to homogeneous isotropic chiral media. It can be applied to a composite with the assumption that the latter can be modeled in terms of an equivalent effective medium, which is what was done in our case; this aspect will be discussed later on. A second comment that has to be made is that our characterization technique is basically a reflection–transmission technique. As a consequence, phenomena such as thickness resonances are potentially present. It can actually be seen that the values of α, $\tan\gamma$, and β are not very much affected by those effects; however, the values of η, ε, and μ can be perturbed in a more important fashion. This will also be discussed further on in this article.

3. Processing and Characterization of Ceramic Helices

3.1 The $(Ba,Sr)TiO_3$ *Family Compounds*

Barium Titanate $BaTiO_3$ is a ferroelectric material which emerged in the 1940s. Because of its high dielectric constant of typically several thousand at MHz frequencies, it was soon used in capacitors. The use of $BaTiO_3$ in the form of a ceramic powder provided a greater ease of

processing when compared to single crystals, and allowed the fabrication of thin multilayered dielectric structures, answering the need for a smaller size and a higher capacitance justified by the development of integrated electronics. The high permittivity of barium titanate is due to its ferroelectric character originating from the presence of an unique polar axis in its crystal structure. This situation results in piezoelectric, pyroelectric, and electro–optic properties which made barium titanate a choice material for a wide range of applications. A sufficient temperature increase brings the material into a non–polar state where it loses its ferroelectricity and becomes paraelectric. The phase transformation is characterized by a transition temperature T_c, at which the static permittivity reaches a maximum, called Curie temperature (about 130° C for $BaTiO_3$). T_c can be tuned by partially replacing Ba^{2+} ions by isovalent ions of comparable radii, such as Sr^{2+}. Strontium is a negative Curie point shifter: the substitution of part of the barium ions with strontium ions reduces the Curie temperature. Thus, such compositions as $Ba_{1-x}Sr_xTiO_3$ enable one to adjust T_c below 130° C (for $x = 0.35$, T_c is close to ambient temperature). A consequence of this property is that for a given temperature and a given frequency, the dielectric constant of $Ba_{1-x}Sr_xTiO_3$ materials can also be adjusted by controlling x.

3.2 Processing of Ceramic Springs

In order to work at room temperature with a material presenting a maximal dielectric constant, we chose the composition $Ba_{0.65}Sr_{0.35}TiO_3$. The ceramic powder is prepared by calcination of barium carbonate $BaCO_3$, strontium carbonate $SrCO_3$ and titanium oxide TiO_2 at 800° C for 2 hours and 1180° C for 5 hours. The subsequent powder is then ball–milled for reducing its particle size, before being mixed with an organic medium and ball–milled to form a slurry. The components of the organic medium should be carefully adjusted so that the slurry has the desired properties (viscosity, drying time, ...) compatible with a high powder loading rate. For a powder weight percentage of 70 %, we found a satisfactory combination of organics, including a fast drying solvent, an acrylic binder, a plasticizer, and a dispersant.

Ceramic springs are prepared by coating carbon fibers of a few microns in diameter with the slurry and winding the resulting composite fiber on a circular graphite cylinder. The diameter of the spring is imposed by that of the graphite rod, while its pitch can be adjusted

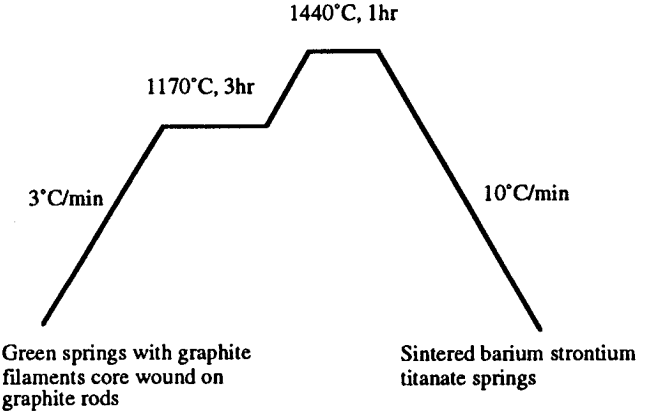

Figure 3. Sintering cycle for the $Ba_{0.65}Sr_{0.35}TiO_3$ springs. The springs are kept at 1170°C for 3 hr in order to eliminate the carbon entirely, and at 1440°C for 1 hr to consolidate the ceramic.

during the winding process. It is worth noticing that straight ceramic fibers can be elaborated by the same method without the winding stage. Once the winding done, the green ceramic helices are heated slowly in order to eliminate the organics comprised in the slurry and the carbon, then maintained at high temperature for densification. The sintering cycle is shown in Fig. 3. There is a probability of incomplete burnout or chemical reactions leading to the presence of undesired secondary phases after sintering. The purity of the ceramic constituting the springs is therefore checked by X–ray diffraction. A typical pattern obtained for crushed barium strontium titanate helices is shown in Fig. 4. No contaminates are found, indicating an efficient burnout of carbon and organics during the heating cycle, and showing the quality of the material. The microstructure was investigated using scanning electron microscopy. Small holes left by the carbon fibers in the central region of the springs cross–section are usually observed, but the overall densification is fairly good for such a simple fabrication process, in particular it is good enough so that the springs can be manipulated. Figure 5 illustrates a variety of ceramic helices susceptible of being made for a given diameter. Throughout our study, we have used the same diam-

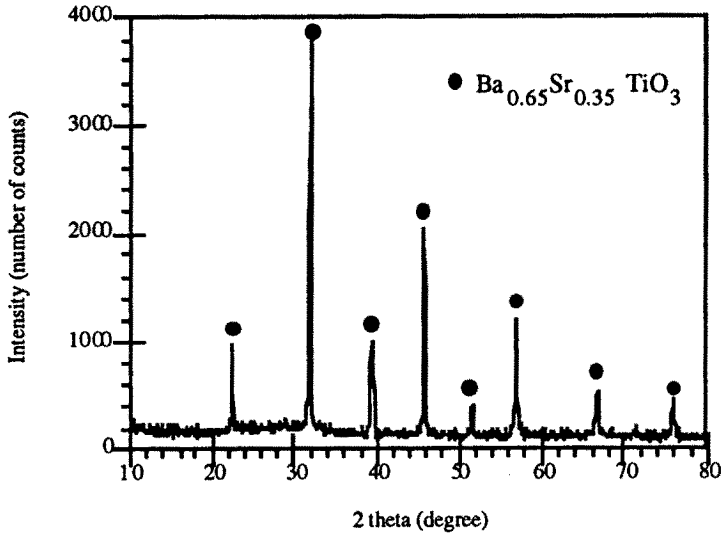

Figure 4. X–ray diffraction pattern obtained for crushed helices. The black dots indicate the location of the reference peaks of $Ba_{0.65}Sr_{0.35}TiO_3$.

eter of 3 mm for all the springs. The latter was imposed by that of the graphite rod on which the winding was made (we consider working with smaller diameters in the future since smaller size rods are now available). The pitch was chosen equal to 3 mm, while the number of turns was either two or three. The average diameter of the fiber itself was approximately 400 microns.

The coating and winding process that we used has the merit of being simple and offering relatively good control over the springs dimensions. More sophisticated methods can be thought of. The one that seems closer to our process is extrusion, much in use for producing superconducting ceramic wires. There is a possibility of extruding either a slurry [26] or ceramic precursors [27]. Another process, substantially more complicated, requires the catalytic pyrolysis of acetylene followed by a vapor phase reaction [28]. This method is interesting because the first stage is the production of carbon helices, which, if they could be made in large enough quantities, could also be attractive for the fabrication of chiral composites. The spring diameters susceptible of being made are as small as a few microns. However, because of the lack of knowledge about their growth mechanism, the morphology of the fibers

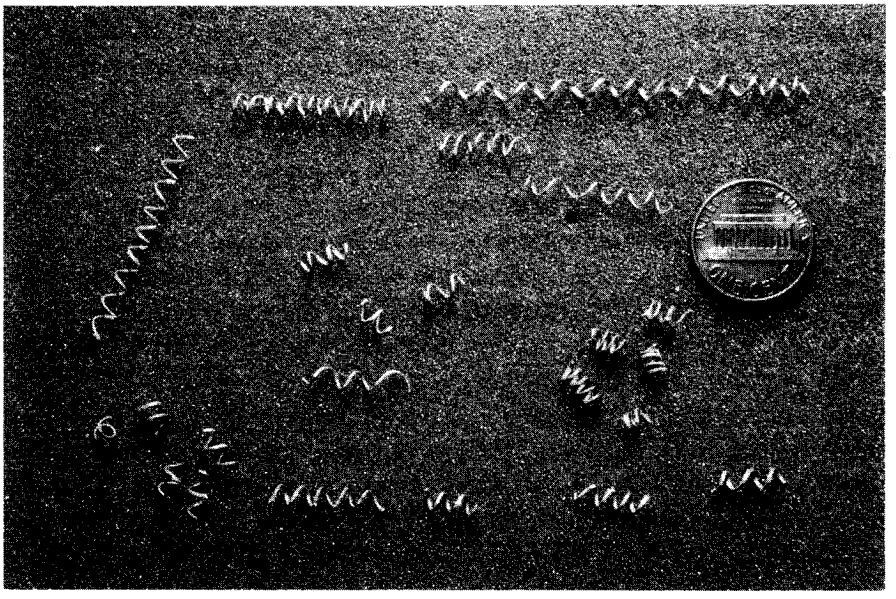

Figure 5. $Ba_{0.65}Sr_{0.35}TiO_3$ **helices of with a common diameter of 3 mm.**

may be difficult to master.

3.3 Electromagnetic Properties Measurements

The dielectric properties of ceramics depend strongly on their microstructure. For various $Ba_{0.65}Sr_{0.35}TiO_3$ ceramic samples, maximum values of the dielectric constant ε_r' of about 6000 and 5300 have been reported at 1 MHz [29, 30]. Larger values can be expected for very well sintered samples, the density of which is closer to the theoretical one. In the same articles and for the same frequency, reported maximum values of the dielectric loss tangent $\tan\delta$ are about 0.017 and 0.04, while values of the Curie temperature are 16° C and 27° C. Measurements at low frequency (typically lower than 10 MHz) are relatively easy to perform on large dielectric constant materials. However, this is not the case in the GHz range. Yet, such measurements are needed, since the dielectric behavior of barium and strontium–based titanates can be significantly modified at high frequencies.

Only a few results are available in the literature on barium strontium titanate. A dielectric constant of about 675 and a loss tangent of about 0.35 at 9.45 GHz and 20° C were reported in 1948 for a polycrystalline $Ba_{0.65}Sr_{0.35}TiO_3$ ceramic [31]. These results can be compared with more recent data obtained with a reflection/transmission method on bulk polycrystalline barium strontium titanate. At 15 GHz, values of 4400 for ε'_r and 0.480 for $\tan\delta$ were reported at ambient temperature for the same composition [32]. It is believed that sample preparation, metallization, and mounting largely influence the results, not to mention the probable differences in the microstructure of the materials, therefore experimental discrepancies can be somewhat large. Errors due to the numerical computation of the dielectric properties from measured values of S–parameters may also play a role. Other measurements performed at ambient temperature for a frequency of 35 GHz on a similar composition with a different permittivity, $Ba_{0.6}Sr_{0.4}TiO_3$, have yielded values around 1950 for ε'_r and 0.2 for $\tan\delta$ [33]. The authors also mention the fact that sample mounting is critical. A ε'_r of 2400 and a $\tan\delta$ of 0.085 were obtained for $Ba_{0.6}Sr_{0.4}TiO_3$ as well at 14.5 GHz [32]. The data of reference 32 and 33 are here in fairly good agreement.

This situation illustrates the difficulty of performing reliable measurements on high permittivity materials in the gigahertz range, in which problems relative to the dependence of the properties on the microstructure cumulate with problems due to the measurement technique itself. We are currently developing a cavity and a reflection /transmission method to obtain data between 1 and 20 GHz on bulk ceramics. A technique for characterizing the dielectric properties of fibers and helices is also being studied in order to take into account the particular morphology of the inclusions used in our composites.

3.4 Chiral Composites Elaboration

The composites are prepared by randomly dispersing the sintered springs in a polymer matrix. The base matrix material we used is a thermosetting epoxy resin, Eccogel (also known as Stycast) 1365–90, manufactured by Grace. Eccogel was used as such, or mixed with 8 % carbon powder in weight. All samples were prepared on the same model: their lateral dimensions are 6 in × 6 in. In order to minimize the number of ceramic helices to be made, the latter occupy only the 4 in × 4 in central region, which is enough for testing in our mi-

Sample	Thickness (mm)	Inclusions	Volume concentration (%)	Matrix
E	8.5	No inclusions	0	Epoxy resin
E1LH	8.8	3-turn LH helices	1.7	Epoxy resin
E3LH	8.9	3-turn LH helices	3.4	Epoxy resin
EC3LH	9.1	3-turn LH helices	3.4	Carbon-loaded epoxy resin
E2	5.7	No inclusions	0	Epoxy resin
LH1.8	5.6	2-turn LH helices	1.8	Epoxy resin
RH1.8	5.7	2-turn RH helices	1.8	Epoxy resin
RA1.8	5.7	2-turn LH and RH helices (racemic mixing)	1.8	Epoxy resin

Table 1. Fabrication characteristics of chiral composites. The volume concentration refers to the volume of ceramic material in the matrix, not to the volume of the cylinders that the helices span. Volume concentrations are estimates based on the springs characteristics given in Section 3.2.

crowave focused beam system, at least for most of the frequencies we are interested in. The dispersion stage is somewhat delicate because of the possible collection of the inclusions in the bottom of the mold. To avoid sedimentation, several layers can be used; it is also possible to monitor the viscosity of the resin. The orientation of the springs should be carefully controlled so that a good tridimensional random orientation is obtained, which is difficult to achieve in practice: the springs tend to lay with their axis in the plane of the composite and need to be rearranged after they are poured into the matrix. Finally, the curing process involves a heating at about 120° C for several hours. The various sample characteristics are summarized in Table 1.

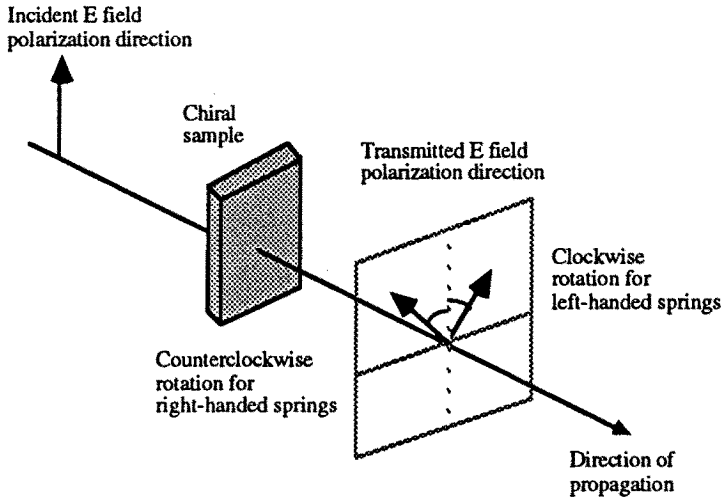

Figure 6. Rotation of the plane of polarization in transmission for left–handed and right–handed springs. The frequency of operation is higher than f_0.

4. Experimental Results and Discussion

4.1 Transmission Properties

4.1.1 Rotation angle and ellipticity

In this section we discuss some properties deduced from transmission measurements: the rotation angle and the ellipticity. The latter two quantities are among the easiest to obtain for a chiral medium, since they are accessible by direct measurement and need, in principle, no use of a particular formalism to be determined. If, however, numerous frequency points are required, it turns out to be more convenient to compute them from S-parameters measurements, as indicated in Section 2.5.

The effect of the handedness of the inclusions on the polarization rotation is shown in Fig. 6. At frequencies higher than the critical frequency f_o mentioned in the introduction, left–handed springs (resp. right–handed springs) make the polarization direction rotate clockwise

Sample	θ at 6 GHz	θ at 6.5 GHz	θ at 7 GHz	θ at 8.6 GHz	θ at 10 GHz	θ at 15.1 GHz	θ at 18 GHz
E2	0°±2°				0.5°CW±0.5°	0°±0.5°	0°±0.5°
LH1.8	6°CCW±3°	2°CW±3°	13°CW±3°	13°CW±3°	14°CW±3°	16°CW±1°	15°CW±1°
RH1.8		0°±2°			16°CCW±2°	14°CCW±2°	15°CCW±1°
RA1.8	3°CW±3°				1°CW±1°	2.5°CW±1°	4°CW±2°

Table 2. Direct measurement of the rotation angle θ for plain epoxy E2, 1.8 vol. % two–turn left–handed helices in epoxy (LH1.8), 1.8 vol. % two–turn right–handed helices in epoxy (RH1.8), and a racemic mixing of left– and right–handed helices in epoxy (RA1.8).

(resp. counterclockwise), as viewed by an observer towards whom the wave is propagating. This result applies to all composites tested so far in our laboratory, whether the inclusions are of metallic or ceramic nature. Measured values of the rotation angle θ are given in Table 2 for two chiral, one racemic, and one achiral samples. These values were obtained by crossing the polarizations of the two antennas of our free–space system, inserting each sample in the measurement cell, and simply rotating the receiving antenna until the minimum transmission is reached again. Because the network analyzer is operated at a single frequency in the continuous sweep mode, the signal stability is not very good and causes some uncertainty in the determination of θ (up to $\pm 3°$).

It can be seen that sample E2, which is made of plain epoxy and is therefore not chiral, yields values very close to 0. LH1.8 and RH1.8, which contain helices of opposite handedness, give opposite rotation angles. Defining the rotatory power ρ as the magnitude of the rotation angle divided by the thickness of the composite, and considering an average rotation of 15° for LH1.8 and RH1.8 between 10 and 18 GHz,

one finds $\rho \approx 1.5°$ mm for a 1% two–turn spring volume fraction at these frequencies. Values of θ measured for RA1.8 are close to 0, as expected for this racemic sample. However, they are somewhat larger than those of plain epoxy, showing than the right– and left–handed spring distribution is not perfectly racemic. RA1.8 actually appears to have a slightly left–handed microstructure in its central region. Results for LH1.8 show that its critical frequency f_o lies between 6 and 6.5 GHz. Below f_o, LH1.8 shows a counterclockwise rotation, while above it presents a clockwise rotation. This behavior is inverted for RH1.8, the critical frequency of which is around 6.5 GHz.

Results regarding values of the rotation angle and the ellipticity obtained via S-parameter inversion with Eqs. (20) for the same four composites are given in Fig. 7. The magnitudes are presented to put emphasis on the comparison between samples with helices of opposite handedness. A good agreement between directly measured and computed values of the rotation angle and f_o can be observed. An underlying assumption in establishing Eqs. (20) being that the effective medium concept applies to the chiral material, this result suggests that, as far as transmission properties are concerned, the modeling described in Section 2 is rather well adapted to our composites.

From the observation of Fig. 7, $|\theta|$ may seem to be almost frequency independent between 8 and 18 GHz for LH1.8 and RH1.8. Nevertheless, a strong dispersion is observed as the frequency is increased above 18 GHz, as can be expected from the empirical model expressed by Eq. (1). Another result worth mentioning is the existence of a frequency at which the ellipticity vanishes and changes sign, the polarization of the transmitted wave being changed from right–elliptically polarized to left– elliptically polarized, or vice–versa. For LH1.8, it is about 15.8 GHz, while for RH1.8, a value close to 14.5 GHz is found. At those particular frequencies, it is possible to transmit a linearly polarized wave through the medium without depolarization.

The frequency at which $|\theta|$ vanishes (the rotation angle θ both vanishes and changes sign, and so does the chirality parameter β, as shown in Eq. (11)), and at which the ellipticity $\tan\gamma$ reaches an extremum can be clearly seen. For LH1.8, θ vanishes and changes sign for a frequency f around 6.3 GHz, while the magnitude of the ellipticity is maximum at about 6.6 GHz. For RH1.8, similar results are obtained. Assuming that the average critical frequency f_o for the two composites is 6.5 GHz, the critical wavelength λ_o in the epoxy matrix

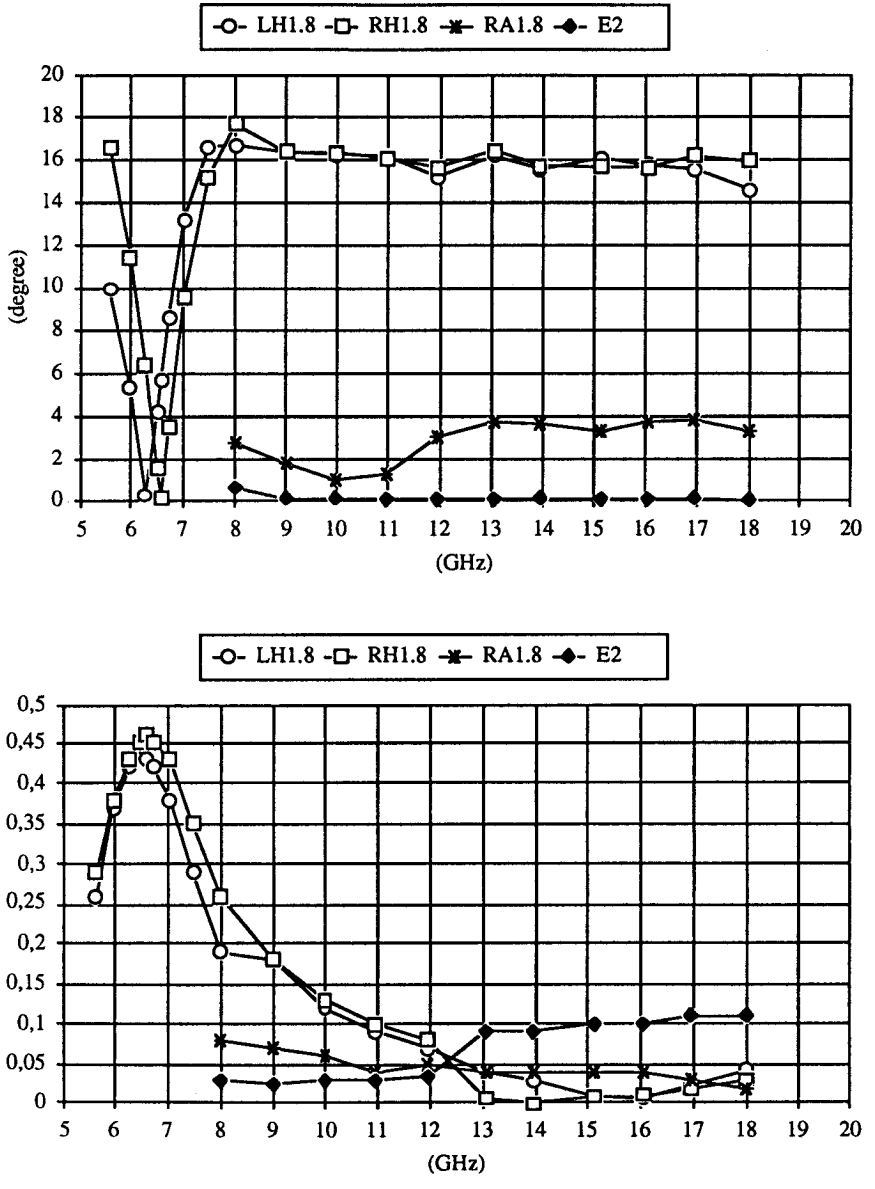

Figure 7. Magnitudes of the rotation angles and the ellipticities of plain epoxy E2, 1.8 vol.% two-turn left-handed helices in epoxy (LH1.8), 1.8 vol.% two-turn right-handed helices in epoxy (RH1.8), and a racemic mixing of left- and right-handed helices in epoxy (RA1.8).

(we assume here $\varepsilon_{epoxy} \approx 3\varepsilon_o$) is 2.66 cm. This value does not agree with the empirical relation $\lambda_{oj} = 2L/j$, where L (about 2 cm) is the stretched length of one inclusion and j is an integer, established for metallic helices and mentioned in the introduction. For $f = f_o$, $|\tan\phi|$ lies around 0.45 for RH1.8, which means that the ratio of the amplitudes of the RCP and LCP waves existing in the chiral medium is larger than 2.5 after propagating through the whole sample.

Regarding samples comprising three–turn springs, we observe average values of $|\theta|$ around 15° for E1LH and 30° for E3LH between 10 and 20 GHz. Values of f_o for E1LH and E3LH have been found to be, respectively around 6 GHz and smaller than 5.8 GHz, which is slightly smaller than what was obtained for two–turn helices and yield values of λ_o which are once again very different from what the empirical rule for metallic helices mentioned above predicts.

4.1.2 Transmission coefficient

The magnitude of the transmission coefficient S_{21}, which is a measure of the magnitude of the copolarized transmitted field, is shown in Fig. 8 for plain epoxy (sample E) and two chiral composites. Thickness resonances are visible for sample E, as well as for sample E1LH, and to a lesser extent, for sample E3LH. The effect of the chiral resonance mentioned in 4.1.1 for E1LH can also be distinguished by the presence of a minimum at around 6 GHz. Assuming that circular dichroism is small (which means working at a frequency far enough from f_o), the magnitude of the total transmitted field in dB can be obtained by adding the quantity $-20\log(\cos\theta)$ to the displayed values, which for $\theta = 30°$ amounts to 1.25 dB.

Using the data presented in Fig. 8 along with reflection data, insertion losses of the chiral composites can be estimated since the thicknesses are known (we consider here that energy is only transmitted in the normal direction, i.e., possible scattering effects are not taken into account). Comparing their values with the only results available so far and obtained for composites containing a comparable volume fraction of metallic inclusions (of smaller size) in the same matrix material [10], it appears that ceramic chiral composites show smaller losses than their metallic counterparts. Studies are currently underway to compare the behavior of composites comprising ceramic and metallic inclusions of identical size in the same matrix material, so that more accurate information can be obtained regarding the influence of the inclusion

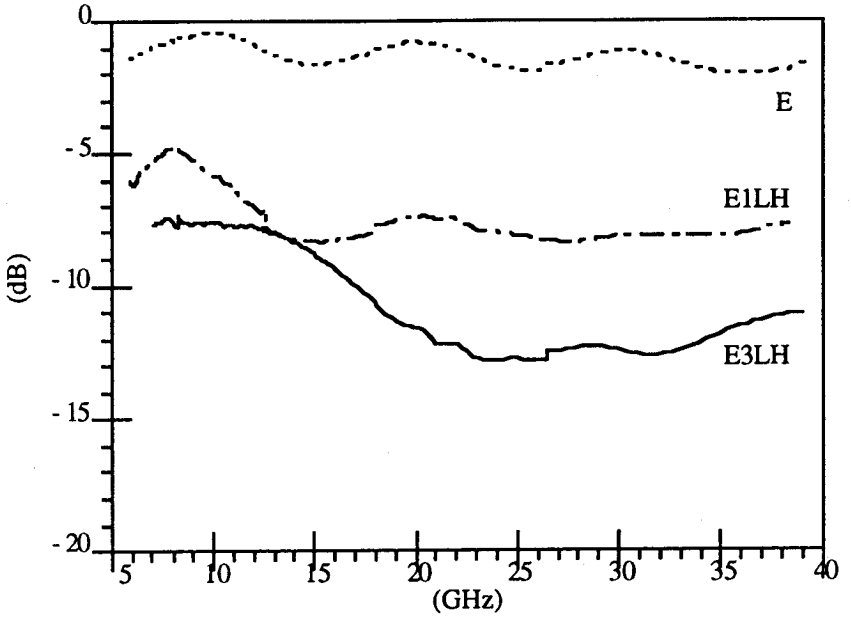

Figure 8. Magnitudes of the copolarized transmitted field for plain epoxy (E), 1.7 vol.% three–turn left–handed helices in epoxy (E1LH), and 3.4 vol.% three–turn left–handed helices in epoxy (E3LH).

material on the transmission losses.

4.2 Reflection Properties

Let us first consider an homogeneous chiral medium. The expression of the normal incidence reflection coefficient for an homogeneous isotropic metal–backed chiral slab given in Eq. (17) can be rewritten as

$$S_{11}^{sc} = \frac{\dfrac{\eta - \eta_o}{\eta + \eta_o} - \mathrm{e}^{2\mathrm{i}k_{eq}d}}{1 - \dfrac{\eta - \eta_o}{\eta + \eta_o}\mathrm{e}^{2\mathrm{i}k_{eq}d}}, \quad \text{with} \quad k_{eq} = \frac{k_L + k_R}{2} = \frac{k}{1 - (k\beta)^2} \tag{22}$$

This relation shows the similarity between the normal incidence reflectivity of chiral and non–chiral media. For a weak chirality $\left((k\beta)^2 \ll 1\right)$,

k_{eq} is almost equal to k, there is therefore no formal difference between the reflectivity of a non–chiral medium and that of a chiral medium. The only advantage that can be thought of lies in the range of values that the permittivity ε and the permeability μ can take, and the possible achievement of a suitable combination of the latter two. If $(k\beta)^2$ is not small compared to 1, then k_{eq} is significantly different from k. In this case, the macroscopic chirality parameter β has in principle, at least from a mathematical standpoint, an influence on the equivalent electrical length of the chiral sample. These considerations apply to normal incidence; however, they are still valid, at least to some extent, for the case of oblique incidence. What should be emphasized is that they are based on the use of the DBF formalism for expressing the constitutive relations that a chiral medium satisfies. If constitutive relations (3) or (4) were used, a more pronounced, or no influence of the chirality parameter on the normal incidence reflectivity would be found [34], but in turn the quantities quantifying chirality in Eqs. (2), (3), and (4) do not have the same meanings and incorporate different kinds of information. Further comments on this particular question are beyond the scope of the present article and are detailed elsewhere in this PIER Book issue [34]. One of the points we would like to make in the following is that even in the DBF (and in the Post-Jaggard) formalism, experimentally achieved values for the chirality parameters do not allow one to consider this variable as a third degree of freedom for the design of absorbent coatings.

Examples provided in the literature can illustrate this discussion. In [7], the influence of the chirality parameter β and the permittivity ε on the reflection from metal–backed chiral coatings was investigated for both normal and oblique incidence. The first two cases (Figs. 1 and 2 of [7]), deal with the dependence of TE and TM reflection efficiencies on β. Computations were made at 100 GHz, for magnitudes of $k\beta$ around the average value of 0.9, which is very large considering the theoretical limit of 1 [10], hereby suggesting that low reflectivity is primarily achieved via a modification of the electrical length of the sample due to chirality. In this situation, there is a dramatic effect on the reflection efficiencies, but the results would have probably been completely different had a smaller frequency (for instance, 10 GHz) or a smaller chirality parameter been chosen.

In [35] and [36], the authors, using the Post-Jaggard formalism, point out that low reflection requirements could be met by impedance

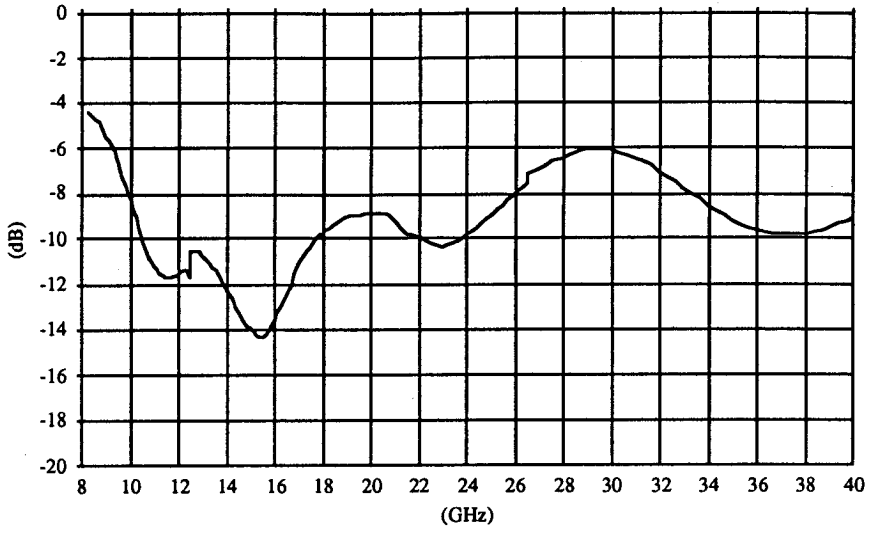

Figure 9. Magnitude of measured S_{11}^{sc} for 3.4 vol.% three–turn left–handed helices in carbon–loaded epoxy (EC3LH).

matching at the front face of the slab through the chirality parameter, along with increased absorption through the chiral skin depths of the LCP and RCP modes. These two conditions can be fulfilled if the two phenomena mentioned above, i.e., a tuning of ε and μ, and a modification of k_{eq} via β occur jointly. In [36], achiral and chiral Dallenbach and Salisbury absorbers of identical dielectric and magnetic properties are compared. The chiral solutions turn out to be more efficient (only normal incidence was studied). However, as in reference [7], neither indication regarding the practical character of the values used for the computations, nor information on the fact that they are physically relevant are given. Let us now consider the case of inhomogeneous chiral materials. If the concept of effective medium applies, then the previous discussion also applies. If not, arguments developed above partially apply, but other phenomena, related to the presence of inclusions, the size of which is comparable to the wavelength in the composite, must also be taken into account.

In Fig. 9, an example of measured normal incidence reflectivity is

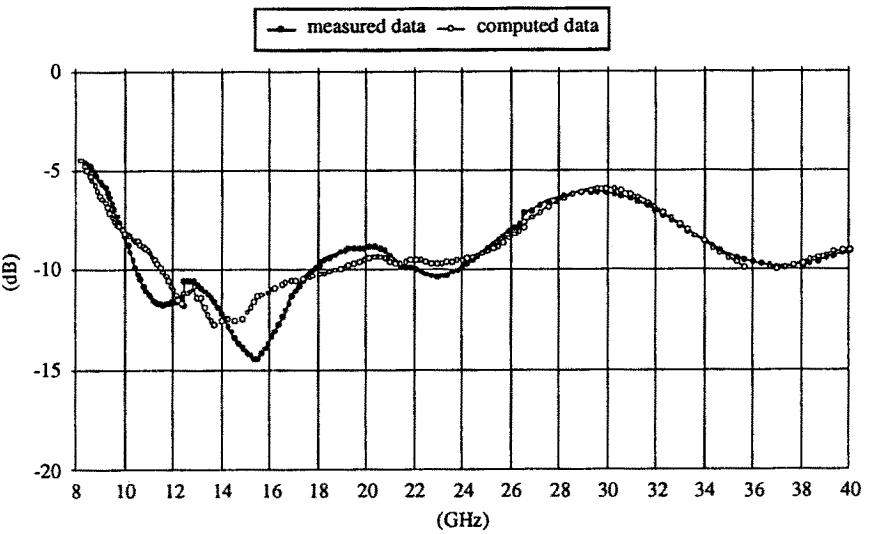

Figure 10. Magnitude of measured and computed S_{11}^{sc} for 3.4 vol.% three-turn left-handed helices in carbon-loaded epoxy (EC3LH).

presented for one of our composites, EC3LH, consisting of a dispersion of three-turn left-handed helices (3.4 % in volume) in carbon-loaded epoxy. The constitutive parameters of this sample (see Section 4.3 for experimental results) were measured using the method indicated in Section 2.5 and used for computing S_{11}^{sc} with Eq. (17). The comparison between measured and computed magnitudes of the normal incidence reflection coefficient of metal-backed EC3LH is shown in Fig. 10. One notices a good agreement between the two curves: the general behaviors as well as the locations of the various minima and maxima are similar. No difference greater than 3 dB is observed. The agreement becomes better as the frequency is increased. Studies on E1LH and E3LH show that it is also improved as the inclusion concentration is increased from 1.7 % to 3.4 % in volume and as carbon is added to the epoxy matrix material. The first and second remarks may be regarded as somewhat non-intuitive. Based on scattering phenomena known for a single target in free-space, one could have expected the agreement to deteriorate both as the frequency was increased (because of hetero-

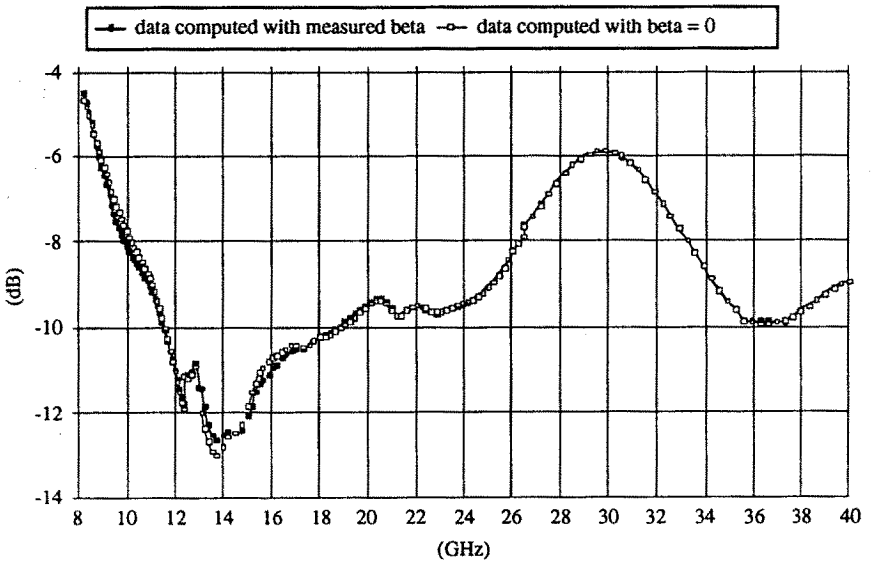

Figure 11. Magnitude of S_{11}^{sc} computed with measured chirality parameter and with zero chirality parameter for 3.4 vol.% three–turn left–handed helices in carbon–loaded epoxy (EC3LH).

geneity effects), and as the concentration was increased (because of a greater interaction between neighboring inclusions). We do not observe this experimentally, suggesting that it may sometimes be erroneous to extrapolate results obtained on a single inclusion to a composite. Moreover, detailed phenomena occurring in a chiral composite have not been fully understood yet. The EM wave can be absorbed in the volume of the inclusions, scattered by the latter, reabsorbed in the matrix material, etc... so that attenuation mechanisms are rather complicated. The helices may also play a special role, acting either as antennas, or guiding the EM wave and "trapping" it in the slab. Naturally, criticisms can be made regarding the validity of defining such quantities as an effective permittivity, permeability, and chirality parameter for a composite like EC3LH, containing helices of several millimeters, and concerning their experimental determination. Rather than starting a theoretical debate, we were more interested in examining if a simple approach could lead to valuable results in terms of chiral composite

reflectivity prediction. Data presented in Fig. 10 show that it is worth being considered. We are currently applying a similar analysis to the case of TE and TM oblique incidences.

In order to gain an understanding of the supposed role of the chirality parameter on achieving low reflectivity, we used the measured values of ε and μ, set β equal to 0, and then computed the corresponding normal incidence reflectivity. By doing this, we simulated an achiral, dielectric and magnetic sample with the same permittivity and permeability as EC3LH. The comparison with the results obtained for the chiral case is shown in Fig. 11. Very little difference is observed between the two curves. This leads to the suggestion that β does not significantly affect k_{eq}. Indeed, for EC3LH we measured absolute values of the real and imaginary parts of β decreasing from about 3×10^{-4} m at 8 GHz to less than 4×10^{-5} m at 30 GHz. The corresponding values for the magnitude of $k\beta$ are approximately comprised between 1×10^{-1} and 2×10^{-1}, hence that of $(k\beta)^2$ is less than $4\ 10^{-2}$, which is not sufficient to have a significant effect on k_{eq}. At this point, we can deduce from the above considerations that in our composites, a low reflectivity is primarily due to a suitable combination of ε and μ.

The normal incidence reflection coefficients of metal-backed composites containing helices of different handedness have been measured. Figure 12 shows results on their magnitudes obtained in the Ku band. It appears that the handedness of the inclusions does not significantly affect $|S_{11}^{sc}|$, although differences arise as one approaches the resonance frequency located beyond 18 GHz, which are believed to primarily originate from small uncertainties in thickness, microstructure and homogeneity resulting from the processing stage. Bearing in mind what was written earlier in this section, we have the confirmation that the magnitude of the chirality parameter (smaller than 4×10^{-4} m in the Ku band for LH1.8 and RH1.8) is too small to have an influence on k_{eq}. Furthermore, given the similarities between the normal incidence reflectivity of the two handed composites LH1.8 and RH1.8, and that of the racemic sample, RA1.8, and considering the differences in the values of their chirality parameters (opposite values were found for LH1.8 and RH1.8, while near-zero values were found for RA1.8), we have an experimental confirmation that the sign of β, i.e., the handedness of the inclusions, does not play a role in the reflectivity behaviors. The controlling factor seems to be, once again, ε and μ, adjusted through the shape of the inclusions. Since the size of the latter is comparable

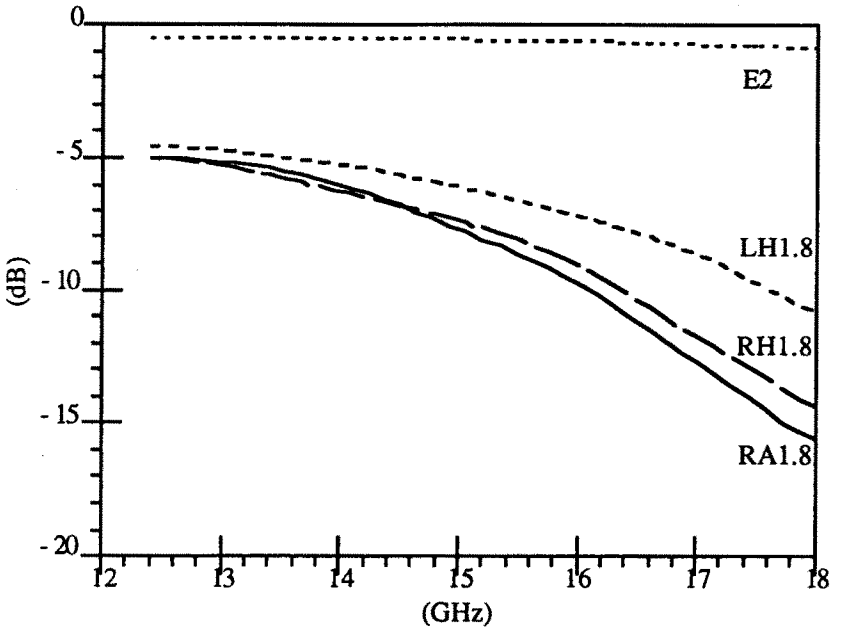

Figure 12. Magnitude of measured S_{11}^{sc} for plain epoxy (E2), 1.8 vol.% two–turn left–handed helices in epoxy (LH1.8), 1.8 vol.% two–turn right–handed helices in epoxy (RH1.8), and a racemic mixing of two–turn springs in epoxy (RA1.8).

with the wavelength, we should qualify those comments by saying that many more experiments are needed in order to quantify additional phenomena and properties that are closely dependent on the heterogeneity of the material, among which are the angular dependence of the reflected energy, the respective importance of diffuse and specular reflection, as well as the loss mechanisms in chiral composites.

The results of Fig. 12 agree with the experimental data obtained by Ro [10] for composites comprising metallic springs, but disagree with those previously reported by Guire et al. (who found a significant difference in reflectivity for samples containing respectively right–handed and a racemic mixing of left– and right–handed metallic springs) [6]. Several remarks can be made to explain this. His composites were much thicker (about 2.7 cm) than ours, hence non–uniformities and dispari-

ties between samples due to the preparation stage could be important. The frequency range of operation was relatively narrow and could have included a resonance peak, around which the reflection coefficient is more dependent on small experimental uncertainties (in addition, the technique used by Guire et al. was the first of its kind: it was by far less accurate than the one used in this study, as well as by Ro). Therefore, it seems reasonable to think that the results obtained here and those found by Ro are more accurate, and conclude that experimentally, little difference between the magnitudes of the reflection coefficients and the reflectivity of composites containing helices of only one handedness and racemic samples is observed. At this point, we would also like to outline that all the comments made in this section are primarily deduced from experiments. It is believed that our understanding will be improved when a satisfactory theory for chiral composites with helical inclusions is worked out.

4.3 Constitutive Parameters

The data presented in this section refer to effective material properties, determined for composites with the assumption that an equivalent homogeneous medium could be associated with each of the samples. It was shown in Section 4.1.1 that, as far as transmission properties were concerned, there was a good chance that the homogeneous medium model was describing our composites appropriately. Because of the analogy between rotation and ellipticity, and real and imaginary parts of the chirality parameter, it can be thought that it is the same for β. Measured values are presented in Fig. 13 for two concentrations of three–turn left–handed springs. The resonant phenomenon observed for θ and $\tan\gamma$ and discussed in Section 4.1.1 can be seen for β' and β'' as well (the value of f_o is about 6.6 GHz for both E1LH and E3LH, showing that there is no influence of the concentration here; for θ and $\tan\gamma$, slightly smaller values of f_o had been found as mentioned in Section 4.1.1), and the dispersive behavior of the chirality parameter can be clearly distinguished. As expected, an inclusion concentration increase leads to an increase in the magnitudes of β' and β'' for frequencies above f_o. Maximum values for the magnitudes of β' and β'' are respectively about 0.65 and 1 mm, which can be compared with data obtained for plain epoxy: $|\beta'|$ and $|\beta''|$ are smaller than 0.01 and 0.02 mm, respectively; the latter values yield an estimate of the accuracy of the method we used.

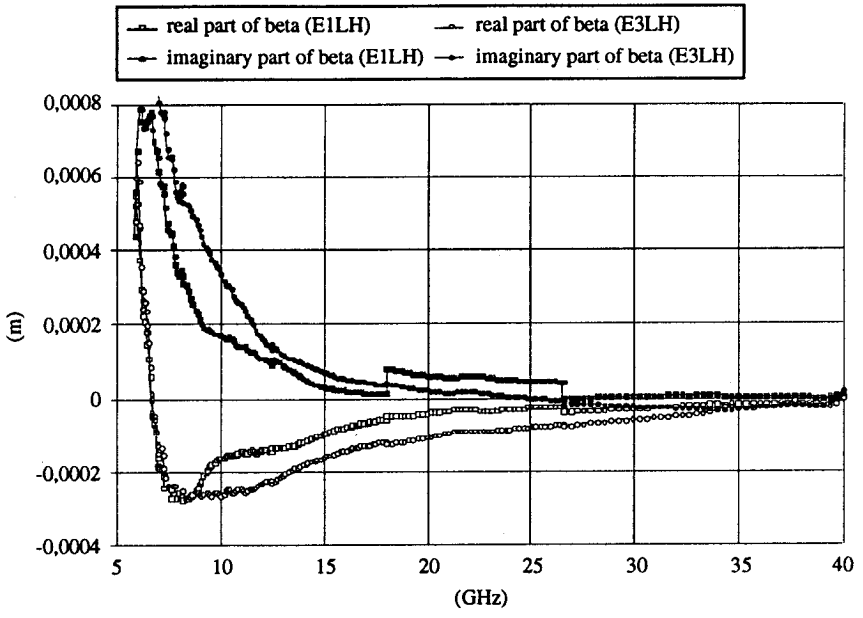

Figure 13. Real and imaginary parts of measured chirality parameter β for 1.7 vol.% three–turn left–handed helices in epoxy (E1LH), and 3.4 vol.% three–turn left–handed helices in epoxy (E3LH).

If the method of determination of the chirality parameter is fairly well adapted to our samples, it may not always be as satisfactory for the relative permittivity and the permeability. First of all, the equivalent homogeneous chiral medium approximation is probably more questionable. In addition, as mentioned in Section 2.5, inaccuracies in the S-parameters inversion due to thickness resonance phenomena unavoidably affect the results in certain frequency ranges. As a consequence, even though it is possible to compute ε and μ for a wide range of frequencies, the obtained values may not always be meaningful and can lead to erroneous conclusions regarding their dispersive behavior, which has a good probability to incorporate parasitic effects. Therefore, rather than presenting broadband data, we chose to give results for discrete frequencies. Values shown in Table 3 were obtained for EC3LH at five frequencies ranging from 18 to 38 GHz. They satisfy energy

Frequency (GHz)	ε_r'	ε_r''	μ_r'	μ_r''	β' (m)	β'' (m)
18	4.59	0.05	1.06	0.45	- 0.0000799	0.0000378
21	4.22	0.13	1.15	0.43	- 0.0000563	0.0000110
30	4.84	0.11	0.54	0.21	- 0.0000393	- 0.0000097
34	3.78	1.07	0.78	0.07	- 0.0000272	- 0.0000095
38	3.40	0.08	0.88	0.30	- 0.0000177	- 0.0000095

Table 3. Experimentally determined constitutive parameters of EC3LH (3.4 vol. % three–turn left–handed helices in carbon–loaded epoxy) for several frequencies.

dissipation requirements (criterion for a passive material) in the DBF formalism [34]. The latter conditions were also double-checked using a second formalism similar to that of Eq. (4). Other results, that we will not mention here for conciseness, were also obtained for LH1.8, RH1.8, and RA1.8. They showed that the relative permittivities and permeabilities of the two handed composites of opposite chirality parameters were very close. The racemic composite also exhibited similar values. Although performing a detailed error analysis is difficult at this stage, disparities are believed to be mainly due to differences in the microstructure originating from the fabrication stage, as indicated in Section 4.2. This is an experimental counterpart of reference 15, where it is shown on a theoretical basis that the permittivity and the permeability being even functions of the chirality parameter, these two variables are equal for a chiral medium and its mirror image. The results agree with those obtained for composites with metallic springs [10]. They also confirm what was previously said on the reflectivity behavior of LH1.8, RH1.8, and RA1.8.

Since all the chiral composites elaborated so far possess some more or less marked heterogeneous character, studies relative to scattering phenomena must be undertaken, not only because they are of primary

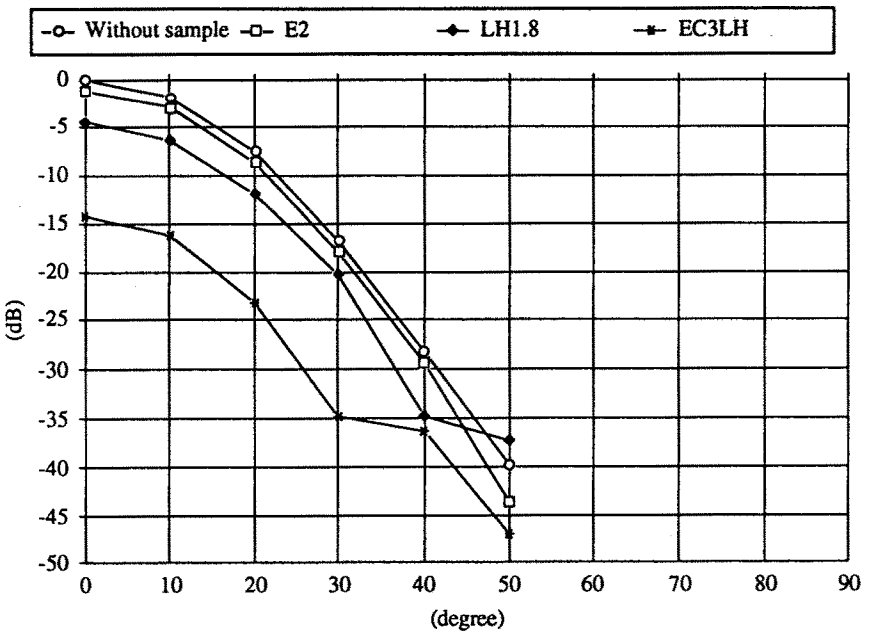

Figure 14. Magnitude of the measured copolarized transmitted field at 10 GHz as a function of the reception angle for four situations: without sample, plain epoxy (E2), 1.8 vol.% two–turn left–handed helices in epoxy (LH1.8), and 3.4 vol.% three–turn left–handed helices in carbon–loaded epoxy (EC3LH).

importance for the knowledge of the performance of the materials as electromagnetic coatings, but also for more fundamental reasons. Figure 14 shows the magnitudes of the copolarized component of the transmitted electric field, as a function of the reception angle (defined as the angle between the incident wave propagation direction, which is normal to the sample surface, and the axis of the receiving horn lens antenna). They were measured at 10 GHz for four different cases: no sample, an homogeneous epoxy sample containing no inclusions (E2), and two composites with ceramic helices (LH1.8 and EC3LH). $|S_{21}|$ was first acquired without sample in the holder of the free–space bench, which yields reference values, then for plain epoxy. For the latter sample, no scattering is expected and the angular response follows that obtained

without sample. For the two composites, departures from this behavior can be observed for angles larger than 30 degrees. Our free–space set-up was not originally designed for performing such measurements, therefore only qualitative comments can be made at this point. Nevertheless, results suggest than some energy is probably radiated along non-specular directions. To which extent this phenomenon affects the various properties measured on chiral composites is not yet known, but this is a first step towards a more detailed characterization of chiral composites.

5. Future Experimental and Theoretical Studies

A lot remains to be done regarding the processing of chiral composites. Metal helices have been used as inclusions, but, to our knowledge, a complete study of the influence of geometrical parameters such as the diameter, the pitch, the wire gauge, or the number of turns on the electromagnetic properties is yet to be carried out. Ceramic inclusions have also appeared. Only one ferroelectric material was tested so far. It seems desirable that other ceramics, among which magnetic materials, be also considered in order to have some idea about the way the properties of the inclusions affect the properties of the composite. For that matter, because the microstructure of an helix is significantly different from that of a bulk sample, specific characterizations of a single inclusion need to be developed. The method for processing the springs also needs some improvements so that a broader range of dimensions be accessible. Other types of inclusions such as chiral polymers or liquid crystals probably deserve some attention as far as the realization of devices is concerned. Another parameter that has not received much consideration is the nature of the matrix material. Attempts were made to use a high temperature cement instead of an epoxy resin, and some high temperature measurements were carried out [37]. Since the constitutive parameters of the matrix are expected to have a strong influence on both transmission and reflection properties of the composites, examining this aspect turns out to be of interest. As a matter of fact, many more composites should be made and tested, not only for evaluating their performances and properties experimentally, but also to provide the research community with some data that can be used for improving the existing theoretical models or creating new ones.

Concerning the reflection/transmission measurements, efforts should be devoted to the method for computing the material parameters from the various S-parameter data. Some work is currently underway to develop a new algorithm for the determination of ε, μ and β, that could avoid such problems as thickness resonance effects. It may also turn out to that some new variables better suited to the description of chiral composites have to be used. Non–classical measurement techniques are being developed. Diffuse transmission experiments are being done at IRCOM; the method is currently being improved so that an adequate characterization of the polarization state of the scattered field be possible. Diffuse reflection measurements are now being performed at Thomson–CSF Central Research Laboratories for composites with and without metal backing. We hope that these experiments will enable us to establish a detailed description of what happens to the incident wave energy, as it interacts with a chiral composite. Another interesting study is to accurately characterize the polarization state of the reflected field (in normal incidence, the reflected field is copolarized with the incident field for an homogeneous chiral sample, and we assumed it was the same for our composites: this could provide another test for the assumption of an equivalent homogeneous medium and a check for scattering effects). We also plan to extend oblique incidence measurements of metal–backed chiral samples and further use them in computer simulations.

Finally, a theoretical model that explicitly takes the microstructure of a chiral composite into account is needed in order to provide some directions for designing materials with specific properties, otherwise the potentialities of chiral materials might never be practically realized. With this goal in mind, a campaign of numerical simulations was recently started in cooperation with Thomson–CSF Radar & Countermeasures Division, for computing the field scattered by an helical inclusion, and study how a composite containing springs could be described. A boundary element method was used and first tried on conducting springs. An adequate post–treatment enabled us to compute the rotation angles and ellipticities of a variety of composites (to be reported elsewhere). This technique is now being applied to non–metallic springs. Figure 15 shows a mesh used for a strontium titanate left–handed helix ($\varepsilon_r' = 300, \tan\delta = 10^{-2}$). The radar cross–sections (RCS) for the copolarized and the crosspolarized components of the scattered field were computed at 10 GHz for various incidences of the

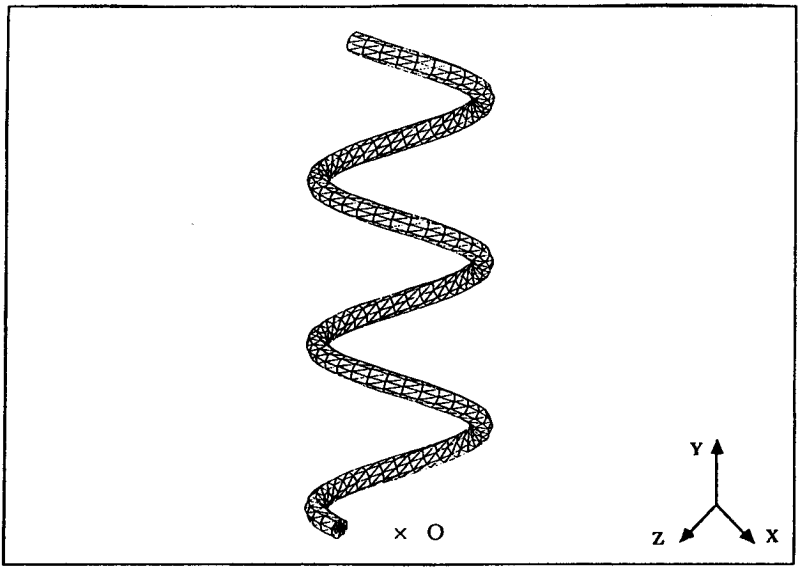

Figure 15. Surface mesh used for boundary element modeling of a $SrTiO_3$ helix at 10 GHz. The external diameter, the pitch, and the wire gauge are respectively equal to 3.4, 3, and 0.4 mm. The helix axis is along the Y direction. The view direction is along [1, 0, 1].

electromagnetic field E: the incident k vector was chosen in the Y - Z plane along the radial direction, and was varied from the positive to the negative Y directions, by steps of 5° (angle χ) while E was normal to k and either in the Y - Z plane along the orthoradial direction or along the X direction. Figure 16 shows the computed results. The copolarized and crosspolarized RCS when E is in the Y - Z plane are maximum for an incidence along the Z direction, and consequently for an electric field direction along that of the helix axis. When the incident electric field is along the X direction, little change with respect to the direction of k is observed for the copolarized RCS (≈ -65 dB.m^2), while the crosspolarized RCS has a maximum for an incidence along Z. It is not our purpose here to further comment on this, which is only

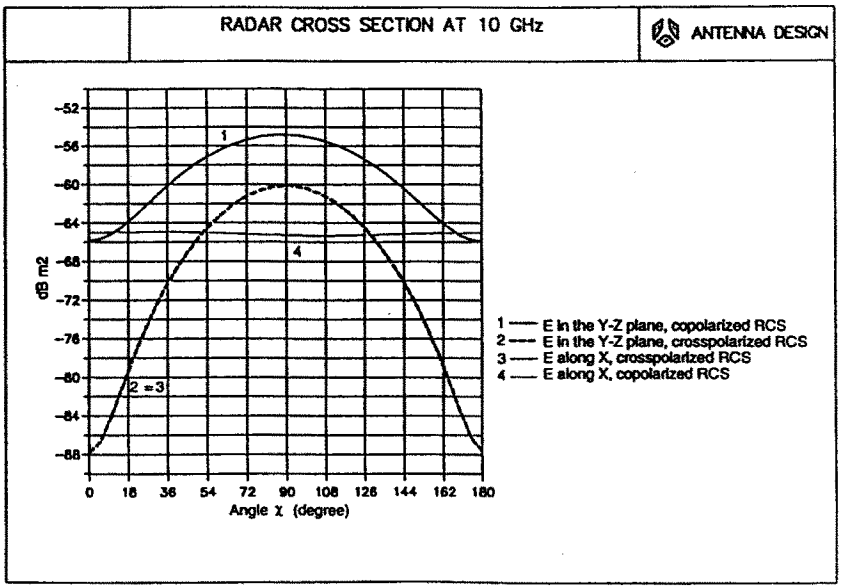

Figure 16. Radar cross-section at 10 GHz for the copolarized and crosspolarized components of the scattered field and several incidences/polarizations. The target is the dielectric helix shown in Fig. 15, suspended in free space. The angle χ is that between the k vector of the incident field and the Y axis.

a preliminary result on the treatment of a dielectric helix as a scattering center in chiral composites. Details will be given in forthcoming publications.

6. Conclusion

We described a method for fabricating ceramic helices and chiral composites containing the latter. The inclusions are of a new kind: previously, only metallic helices had been employed. A free–space technique for measuring the S-parameters and reflectivities of chiral samples was presented. Assuming that the concept of equivalent homogeneous medium applied to our composites, the various transmission properties and constitutive parameters were deduced from a set of normal incidence experiments. The resonant behaviors of the rotation angle and the chirality parameter were investigated. The reflectivities of homogeneous and inhomogeneous chiral media were analyzed in some detail, and results concerning composites were given. Values of the effective permittivity and permeability were also presented, and some problems relative to their determination, discussed. Non–classical experiments aiming at characterizing scattering effects in chiral composites were introduced. Such a class of measurements will take a larger place in future experiments. Finally, a method for modeling chiral composites based on the interaction of an EM wave with chiral helical inclusions was mentioned, and preliminary results were shown.

Acknowledgments

Part of this work was made at the Pennsylvania State University, Department of Engineering Science and Mechanics, Center for the Engineering of Electronic and Acoustic Materials, under a financial grant from Thomson–CSF. The author wishes to thank Pr. V. K. Varadan, Pr. V. V. Varadan, and Pr. Y. Ma from Penn State, as well as Dr. J. P. Ganne, Dr. M. Labeyrie, and Dr. P. Bannelier from Thomson–CSF for fruitful discussions and advices. Pr. P. Y. Guillon, P. Vigier, and H. Jallageas from IRCOM, University of Limoges, are also acknowledged.

References

1. Varadan, V. K., and V. V. Varadan, "Electromagnetic shielding and absorptive materials," U.S. Patent No. 4,948,922, 1990.
2. Engheta, N., and D. L. Jaggard, "Waveguides using chiral materials," U.S. patent No. 5,165,059, 1992.

3. Lindmann, K. L., "Uber eine durch ein isotropes System von spiralformigen Resonatoren erzeugte Rotationspolalisation der elektromagnetischen Wellen," Annalen der Physik, Vol. 63, No. 4, 621–644, 1920.
4. Winkler, M. H., "An experimental investigation of some models for optical activity," *J. Phys. Chem.*, Vol. 60, 1665–1668, 1956.
5. Tinoco, I., and M. P. Freeman, "The optical activity of oriented copper helices: I. Experimental," *J. Phys. Chem.*, Vol. 61, 1196–1200, 1957.
6. Guire, T., V. K. Varadan, and V. V. Varadan, "Influence of chirality on the response of EM waves by planar dielectric slabs," *IEEE Trans. Elec. Comp.*, Vol. 32, No. 4, 300–303, 1990.
7. Varadan, V. K., V. V. Varadan, and A. Lakhtakia, "On the possibility of designing anti–reflection coatings using chiral composites," *J. Wave–Mat. Int.*, Vol. 2, No. 1, 71–81, 1987.
8. Umari, M. H., V. K. Varadan, and V. V. Varadan, "Rotation and dichroism associated with microwave propagation in chiral composites," *Radio Science,* Vol. 26, No. 2, 1327–1334, 1991.
9. Ro, R., V. K. Varadan, and V. V. Varadan, "Electromagnetic activity and absorption in microwave chiral composites," *IEE Proceedings–H,* Vol. 139, No. 5, 441–448, 1992.
10. Ro, R., "Determination of the electromagnetic properties of chiral composites using normal incidence measurements," Ph.D Thesis, The Pennsylvania State University, Engineering Science and Mechanics, 1991.
11. Hollinger, R. D., V. V. Varadan, D. K. Ghodgaonkar, and V. K. Varadan, "Experimental characterization of isotropic chiral composites in circular waveguides," *Radio Science,* Vol. 27, No. 2, 161–168, 1992.
12. Bohren, C. F., "Angular dependence of the scattering contribution to circular dichroism," *Chem. Phys. Lett.*, Vol. 40, No. 3, 391–396, 1976.
13. Post, E. J., *Formal Structure of Electromagnetics,* North–Holland, Amsterdam, 1962.
14. Jaggard, D. L., X. Sun, and N. Engheta, "Canonical sources and duality in chiral media," *IEEE Trans. Ant. Prop.*, Vol. 36, No. 7, 1007–1013, 1988.
15. Sihvola, A. H., and I. V. Lindell, "Bi–isotropic constitutive relations," *Micro. Opt. Tech. Lett,* Vol. 4, No. 8, 295–297, 1991.

16. Bohren, C. F., "Light scattering by an optically active sphere," *Chem. Phys. Lett.*, Vol. 29, No. 3, 458–462, 1974.
17. Eftimiu, C., and Pearson, L. W., "Guided electromagnetic waves in chiral media," *Radio Science,* Vol. 24, No. 3, 351–359, 1989.
18. Engheta, N., and P. Pelet, "Modes in chirowaveguides," *Optics Lett.,* Vol. 14, No. 11, 593– 595, 1989.
19. Viitanen, A. J., and I. V. Lindell, "Perturbation theory for a corrugated waveguide with a bi–isotropic rod," *Micro. Opt. Tech. Lett.,* Vol. 5, No. 14, 729–732, 1992.
20. Tretyakov, S. A., and A. J. Viitanen, "Perturbation theory for a cavity resonator with a bi–isotropic sample: applications to measurements techniques," *Micro. Opt. Tech. Lett.,* Vol. 5, No. 4, 174–177, 1992.
21. Ougier, S., I. Chenerie, and S. Bolioli, "Measurement method for chiral media," *Proc. 22nd European Microwave Conference,* Vol. 1, Helsinki, Finland, 682–687, 1992.
22. Bassiri, S., C. H. Papas, and N. Engheta, "Electromagnetic wave propagation through a dielectric–chiral interface and through a chiral slab," *J. Opt. Soc. Am.,* Vol. 5–A, No. 9, 1450– 1459, 1988.
23. Ghodgaonkar, D. K., V. V. Varadan, and V. K. Varadan, "A free–space method for measurement of dielectric constants and loss tangents at microwave frequencies," *IEEE Trans. Instrum. Meas.,* Vol. 37, No. 3, 789–793, 1989.
24. Ghodgaonkar, D. K., V. V.,Varadan, and Varadan, V. K., "Free–space measurement of complex permittivity and complex permeability at microwave frequencies," *IEEE Trans. Instrum. Meas.,* Vol. 39, No. 2, 387–394, 1990.
25. Varadan, V. V., R. D. Hollinger, D. K. Ghodgaonkar, and V. K. Varadan, "Free–space, broadband measurements of high temperature, complex dielectric properties at microwave frequencies," *IEEE Trans Instrum. Meas.,* Vol. 40, No. 5, 842–846, 1991.
26. Dorris, E. S., J. T. Dusek, M. T. Lanagan, J. J. Picciolo, J. P. Singh, J. E. Creech, and R. B. Poeppel, "Extrusion of Multilayer Superconductor Coils," *Ceram. Bull.,* Vol. 70, No. 4, 722–726, 1991.
27. Katayama, S., and M. Sekine, "Fabrication of superconducting $YBa_2Cu_3O_{7-x}$ fibers by the sol–gel method using metal alkoxides," *J. Mater. Res.,* Vol. 6, No. 8, 1629–1633, 1991.

28. Motojima, S., M. Kawaguchi, K. Nozaki, and H. Iwanaga, "Preparation of coiled ceramic fibers by CVD," *Proceeding of the* 11^{th} *International Conference on Chemical VaporDeposition,* The Electrochemical Society, 573–579, 1990.
29. Selmi, F., F. Guerin, X. D. Yu, V. K. Varadan, and V. V. Varadan, "Microwave calcination and sintering of barium strontium titanate," *Mater. Lett.,* Vol. 12, No. 6, 424–428, 1992.
30. Varadan, V. K., D. K. Ghodgaonkar, V. V. Varadan, J. F. Kelly, and P. Glikerdas, "Ceramic phase shifter for electronically steerable antenna systems", *Microwave J.,* 116–127, January 1992.
31. Powles, J. G., "Dielectric properties of mixed barium and strontium titanates at 10,000 Mcs," *Nature,* No. 4121, 655, 1948.
32. Ghodgaonkar, D. K., R. Hughes, F. Selmi, V. V. Varadan, and V. K. Varadan, "Ferroelectric phase shifters for electronically steerable antenna systems," *Proc. 1992 Joint Symposia IEEE-APS/ URSI/NEM Meeting,* Chicago, 272–275, 1992.
33. Burdick, G. A., T. J. Lyon, and J. E. Pippin, "Measurements of large dielectric constants and loss tangents at 35 Gc/s," *IEEE Trans. Instrum. Meas.,* 318–325, December 1964.
34. Guerin, F., "Energy dissipation and absorption in reciprocal biisotropic media described by different formalisms," in this issue.
35. Jaggard, D. L., and N. Engheta, "Chirosorb as an invisible medium," *Electron. Lett.,* Vol. 25, No. 3, 173–174, 1989.
36. Jaggard, D. L., N. Engheta, and J. Liu, "Chiroshield: a Salisbury/Dallenbach alternative," *Electron. Lett.,* Vol. 26, No. 17, 1332–1334, 1989.
37. Guerin, F., V. K. Varadan, and V. V. Varadan, "Processing and microwave characterization of chiral composites containing ferroelectric ceramic inclusions," *1992 Joint Symposia IEEE-APS/ URSI/NEM Meeting,* Chicago, USA, July 18–25, 1992.